Manuscript prepared for J. Name
with version 4.2 of the LaTeX class copernicus.cls.
Date: 11 July 2012

A comprehensive approach to analyze discrepancies between land surface models and in-situ measurements: a case study over US and Illinois with SECHIBA forced by NLDAS

M. Guimberteau[1], A. Perrier[2], K. Laval[1], and J. Polcher[1]

[1]Laboratoire de Météorologie Dynamique (LMD), UMR8539 – CNRS, Vincent Cassé, Palaiseau, 05: Ile-de-France Ouest et Nord, Paris, France
[2]AgroParisTech, UFR Physique de l'Environnement, Paris, France

Correspondence to: M. Guimberteau (matthieu.guimberteau@upmc.fr)

Abstract. The purpose of this study is to test the ability of the Land Surface Model SECHIBA to simulate water budget and particularly soil moisture at two different scales: regional and local. The model is forced by NLDAS data set at 1/8th degree resolution over the 1997–1999 period. SECHIBA gives satisfying results in terms of evapotranspiration and runoff over US compared with four other land surface models, all forced by NLDAS data set for a common time period. The simulated soil moisture is compared to in-situ data from the Global Soil Moisture Database across Illinois by computing a soil wetness index. A comprehensive approach is performed to test the ability of SECHIBA to simulate soil moisture with a gradual change of the vegetation parameters closely related to the experimental conditions. With default values of vegetation parameters, the model overestimates soil moisture, particularly during summer. Sensitivity tests of the model to the change of vegetation parameters are performed and show that the roots extraction parameter has the largest impact on soil moisture, others parameters such as LAI, height or soil resistance having a minor impact. Moreover, a new computation of evapotranspiration including bare soil evaporation under vegetation has been introduced into the model. The results point out an improvement of the simulation of soil moisture when this effect is taken into account. Finally, soil moisture sensitivity to precipitation variation is addressed and it is shown that soil moisture observations can be rather different depending on the method to measure field capacity. When the observed field capacity is deducted from the observed volumetric water profiles, simulated soil wetness index is closer to the observations. Excepted for one station, the monthly mean correlation is around 0.9 between observations and simulation.

1 Introduction

Land Surface Models (LSMs) are designed to simulate surface conditions with vegetation and soil parameters that are calibrated at global scale. However, many studies focus on regional scale for model validation or climate change impacts. It is therefore reasonable to ask if the parameters of the LSMs are able to represent surface conditions in agreement with local measurements. Thus, a comprehensive approach is performed in this study focused on water budget simulation at large scale over the US and particulary on soil moisture content at local scale over Illinois (Fig. 1). Soil moisture is a crucial component of the water cycle. It strongly influences the partition of surface fluxes between latent and sensible heat. It impacts on evapotranspiration (ET) and consequently on the turbulent fluxes into the boundary layer and also on surface runoff. In climate simulations using LSM coupled to Global Circulation Model (GCM), the capture of the variation of soil moisture state during the year is important in order to have realistic feedback between continental surface and atmosphere. Many works have focused on the sensitivity of LSMs fluxes to soil moisture (Dirmeyer et al., 2000). The aim of this paper is to give an overview of the validity of three water cycle components simulated by the LSM SECHIBA (Schématisation des EChanges Hydriques à l'Interface Biosphère-Atmosphère, Ducoudré et al., 1993) at different spatial scales: ET, total runoff and soil moisture. Over the US, the first two are compared with results of LSMs forced by the same North american Land Data Assimilation System (NLDAS, Cosgrove et al., 2003) forcing dataset, at 1/8th degree spatial resolution over 1997–1999 period. Then, we focus over a smaller region of the US, the state of Illinois (Fig. 1), where in-situ soil moisture measurements have been performed and merged into a database by Robock et al. (2000). These observations are available for the studied time period (i.e. 1997–1999) and allow us to evaluate the SECHIBA results for simulated soil moisture. The ability of the LSM SECHIBA to simulate monthly variation of soil moisture is highlighted through a gradual and comprehensive adjustement of the parameters of the vegetation (LAI, root extraction, height). The impacts of the change of the parameters on simulated soil moisture are studied. Then, the uncertainties of dataset to assess the validity of the simulation are analysed. The role of precipitation rate during the studied period and the significance of defining field capacity are highlighted.

2 Forcing data set and model

2.1 NLDAS forcing data set

NLDAS forcing dataset used to force the model covers all the United States and a part of Canada and Mexico. The time resolution is hourly and the latitude-longitude spatial resolution is of 1/8th degree which is quite high compared to the current forcing resolution for LSMs generally around half degree. This high resolution is useful to investigate land surface processes at regional scales with better confidence and it is therefore suitable for this study. NLDAS data set is a combination of Eta

Data Assimilation System (EDAS) models outputs, observation-based precipitation and shortwave radiation data. Precipitation forcing was built with Stage II hourly Doppler Radar and River Forecast Center gauge data (Baldwin and Mitchell, 1997), Climate Prediction Center (CPC) daily gauge data (Higgins et al., 2000) and reprocessed daily gauge data. Observed shortwave values are derived from Geostationary Operational Environmental Satellite (GOES) radiation data processed at the University of Maryland and at the National Environmental Satellite data and Information Service (Pinker et al., 2003). The nine primary forcing fields of the forcing used for this study are summed up in Table 1.

Precipitation is one of the most important forcing variables due to its strong impact on soil water budget and consequently on soil moisture content seasonality. In NLDAS, precipitation data comes from a combination of model outputs and observations. Therefore, differences can be found with in-situ data results which can be important for regional scale simulations. In this study, NLDAS precipitation is compared with in-situ observations from 16 Illinois Climate Network (ICN) stations averaged over Illinois, during the time period 1997–1999. The mean annual value of NLDAS precipitation is 2.73 $\mathrm{mm\,d^{-1}}$ over the period, 12 % higher than observations (2.44 $\mathrm{mm\,d^{-1}}$). The highest overestimation occurs during spring and early summer (Fig. 2a). The overestimation is quasi-systematic during all the three years (Fig. 2b). However, NLDAS precipitation variation is quite satisfying (linear correlation is about 0.97) where the wet summer in 1998 and the dry autumn in 1999 are well captured.

2.2 Model description

SECHIBA is the hydrological module of the LSM ORCHIDEE (ORganising Carbon and Hydrology In Dynamic EcosystEms), a model of the Pierre Simon Laplace Institute (IPSL), used to simulate the hydrological exchanges between soil, vegetation and atmosphere at a time-step of Δt = 30 min.

2.2.1 Vegetation and LAI

In each grid-cell, up to twelve Plant Functional Types (PFTs) can be represented simultaneously (plus bare soil), prescribed by the 1 km global land cover map (International Geosphere Biosphere Programme (IGBP), Belward et al., 1999) reduced by a dominant-type method to 5 km spatial resolution with the Olson classification (Olson et al., 1983). Maximal fraction of vegetation v ($f_{\mathrm{v}}^{\max}$) is thus defined for each grid cell. It is modulated by the Leaf Area Index ($\mathrm{LAI_v}$) growth, specific for each PFT represented in the model, giving the fraction of vegetation f_{v}:

$$f_{\mathrm{v}} = f_{\mathrm{v}}^{\max} \min(2\mathrm{LAI_v}, 1) \tag{1}$$

The fraction of bare soil ($\mathrm{v} = 1$) increases linearly as much as the decrease of the other fractions

of vegetation ($2 \leq \mathrm{v} \leq 13$) with a LAI lower than 0.5:

$$f_1 = f_1^{\max} + \sum_{\mathrm{v}=2}^{13} (f_{\mathrm{v}}^{\max} - f_{\mathrm{v}}) \tag{2}$$

where $f_1^{\max}$ is the maximal fraction of bare soil.

The main method to simply simulate the LAI in the model, is to prescribe it by a map (Belward et al., 1999) whose values come from Normalized Difference Vegetation Index (NDVI) observations. We have chosen to compute the LAI depending on the variation of soil temperature at 50 cm depth (T_{soil} in K) (Polcher, 1994) which has a smoothed seasonality during the year. This parameterization has been recently used in the model for a better seasonality of LAI for numerical experiments which simulates irrigation with SECHIBA (Guimberteau, 2006, 2010) and this method has been selected for our study. LAI growth is bounded by a minimal ($\mathrm{LAI}_{\mathrm{v}}^{\min}$) and a maximal value ($\mathrm{LAI}_{\mathrm{v}}^{\max}$) of LAI. Between these limits, LAI growth depends on the variation of soil temperature at 50 cm depth during the year, bounded by minimal ($T_{\mathrm{soil_v}}^{\min}$) and maximal values ($T_{\mathrm{soil_v}}^{\max}$) of soil temperature at 50 cm depth (both in K) that can be different according to the PFT considered (Guimberteau, 2006, 2010):

$$\mathrm{LAI}_{\mathrm{v}} = \mathrm{LAI}_{\mathrm{v}}^{\min} + f(T_{\mathrm{soil_v}}) \left(\mathrm{LAI}_{\mathrm{v}}^{\max} - \mathrm{LAI}_{\mathrm{v}}^{\min} \right) \tag{3}$$

where $f(T_{\mathrm{soil_v}})$ (in K) is the function of growth of LAI for the PFT according to the soil temperature at 50 cm depth:

$$f(T_{\mathrm{soil_v}}) = \left[1 - \left(\frac{T_{\mathrm{soil_v}}^{\max} - T_{\mathrm{soil}}}{T_{\mathrm{soil_v}}^{\max} - T_{\mathrm{soil_v}}^{\min}} \right)^2 \right] \tag{4}$$

2.2.2 Soil hydrology

Soil moisture in SECHIBA model is defined for this study. This hydrological scheme is described in detailed in Ducoudré et al. (1993) and D'Orgeval (2006). The two meters ($h_{\mathrm{tot}} = 2\mathrm{m}$) soil column is represented by two moisture layers (Fig. 3), a superficial one subjected to strong ET and root extraction, and a deep one only related to deep root extraction. The first layer has a thickness smaller than the lowest one and its height (h_{upper} in m) varies because it interacts strongly with the atmosphere. Consequently, the soil moisture of the superficial layer q_{upper} is directly controlled by the moisture convergence:

$$\frac{\mathrm{d}}{\mathrm{d}t} q_{\mathrm{upper}} = P - E - D \tag{5}$$

where q_{upper} ($\mathrm{kg m^{-2}}$) is the amount of water available for the plants in the upper reservoir, $P = \mathrm{Rainf} + \mathrm{Snowf}$ ($\mathrm{kg m^{-2} s^{-1}}$) is precipitation, E ($\mathrm{kg m^{-2} s^{-1}}$) the total ET (that is to say the sum of water loss through bare soil evaporation, evaporation of water intercepted by the vegetation, transpiration of the cover and sublimation), and D ($\mathrm{kg m^{-2} s^{-1}}$) the drainage between the two soil layers (Ducharne et al., 1997; Dümenil and Todini, 1992; Rowntree and Lean, 1994).

The hydrological budget is computed for each PFT within the mesh and then averaged over the grid cell. With this bucket model, we assume that surface runoff and deep drainage are produced only when soil reaches field capacity (when $q_{\rm upper} + q_{\rm lower} > q_{\rm tot}$ where $q_{\rm lower}$ ($\rm kg m^{-2}$) is the amount of water available for the plants in the lower reservoir and $q_{\rm tot}$ ($\rm kg m^{-2}$) the maximum amount of water that vegetation can extract from the soil). In the model, the total water excess is prescribed as: 95 % in deep drainage ($\rm kg m^{-2} s^{-1}$) and 5 % in surface runoff R ($\rm kg m^{-2} s^{-1}$).

The Soil Wetness Index (SWI) is used to describe the state of soil moisture and is useful to compare the different LSMs outputs (Dirmeyer et al., 2000) but also in-situ observations (Saleem and Salvucci, 2002). This index presented here is used in our study to compare SECHIBA outputs and observations data. SWI gives a simple representation of the water stress for the vegetation and indicates the actual available soil water for plants at each time. SWI ranges between 0 (lower this value, no more soil water can be extracted by the roots) to 1 (upper this value, no more water can be retained by the soil over some days):

$$\mathrm{SWI} = \frac{W - W_{\rm wilt}}{W_{\rm fc} - W_{\rm wilt}} \tag{6}$$

where W ($\rm kg m^{-2}$) is the actual equivalent water depth stored in the soil, $W_{\rm wilt}$ ($\rm kg m^{-2}$) the equivalent water depth at the wilting point of the soil (determined by the soil and the vegetation properties) and $W_{\rm fc}$ ($\rm kg m^{-2}$) the field capacity (based on soil texture alone) which represents the retained water in a natural soil after gravitation action.

The simulated SWI can be computed from the weighted average of the composite amount of water available for the plants into each PFT reservoir:

$$\mathrm{SWI}_{\rm ORCH} = \frac{q_{\rm upper} + q_{\rm lower}}{q_{\rm tot}} \tag{7}$$

where $q_{\rm tot}$ is obtained by integrating the maximal soil water amount per unit of soil volume ($w_{\rm max} = 150 \rm kg m^{-3}$):

$$q_{\rm tot} = h_{\rm tot} w_{\rm max} \tag{8}$$

2.2.3 Evapotranspiration and root extraction

Evapotranspiration computation in the initial version of SECHIBA

ET is a sum of four components: evaporation of water intercepted by the cover ($I_{\rm v}$ in $\rm kg m^{-2} s^{-1}$), transpiration of vegetation ($T_{\rm v}$ in $\rm kg m^{-2} s^{-1}$), bare soil evaporation (E_1 in $\rm kg m^{-2} s^{-1}$), and sublimation of snow (not detailed here).

In the initial version of SECHIBA, the intercepted water is evaporated on the wet fraction of the cover, ($F_{\rm wet}$, Eq. 9), which is the ratio between the amount of water (i.e. precipitation P) received by the leaf ($x_{\rm v} = f_{\rm v} P \Delta$t, $\rm kg m^{-2}$) and the maximal amount of intercepted water ($x_{\rm v}^{\rm max}$ in $\rm kg m^{-2}$). The latter depends on the LAI and a coefficient $\alpha = 0.1$ that converts LAI into size of interception loss reservoir (Eq. 10).

$$F_{\rm wet} = \frac{x_{\rm v}}{x_{\rm v}^{\rm max}} \tag{9}$$

$$x_{\rm v}^{\rm max} = \alpha f_{\rm v} {\rm LAI}_{\rm v} \tag{10}$$

The evaporation of water intercepted by the cover ($I_{\rm v}$, Eq. 11) takes into account the structural (or architectural) resistance ($r_{\rm s_v}$ in $\rm sm^{-1}$), and the aerodynamic resistance ($r_{\rm a}$ in $\rm sm^{-1}$).

$$I_{\rm v} = \min\left[X_{\rm v}, f_{\rm v} F_{\rm wet}\left(\frac{1}{1+\frac{r_{\rm s_v}}{r_{\rm a}}}\right) E_{\rm pot}\right] = \min\left[X_{\rm v}, I_{\rm v}^{\rm max}\right] \tag{11}$$

where $X_{\rm v} = f_{\rm v} P$ ($\rm kgm^{-2}s^{-1}$) is the flux of water intercepted by the cover, $E_{\rm pot}$ ($\rm kgm^{-2}s^{-1}$) the potential evaporation (Budyko, 1956) and $I_{\rm v}^{\rm max}$ ($\rm kgm^{-2}s^{-1}$) the maximal evaporation of water intercepted by the cover.

At the same time, on the dry fraction of the leaves surfaces ($F_{\rm dry}$, Eq. 12), transpiration ($T_{\rm v}$, Eq. 13) is computed. Transpiration is function of the canopy resistance (including both bulk stomatal and leaf aerodynamic resistances, $r_{\rm sto_v}$ in $\rm sm^{-1}$) and the root extraction potential $U_{\rm s_v}$ (De Rosnay and Polcher, 1998) which reproduces the ability of roots to extract water (detailed next).

$$F_{\rm dry} = 1 - \left(\frac{x_{\rm v}}{x_{\rm v}^{\rm max}}\right) \tag{12}$$

$$T_{\rm v} = f_{\rm v} F_{\rm dry}\left(\frac{1}{1+\frac{r_{\rm s_v}+r_{\rm sto_v}}{r_{\rm a}}}\right) U_{\rm s_v} E_{\rm pot} \tag{13}$$

Bare soil evaporation (E_1, Eq. 14), is computed through a resistance (r_1 in $\rm sm^{-1}$, Eq. 15), proportional to the relative dryness of the upper soil layer ($h_{\rm upper_1}^{\rm dry}$ in m).

$$E_1 = f_1\left(\frac{1}{1+\frac{r_1}{r_{\rm a}}}\right) U_{\rm s_1} E_{\rm pot} \tag{14}$$

$$r_1 = h_{\rm upper_1}^{\rm dry} r_{\rm soil} \tag{15}$$

where $r_{\rm soil}$ ($\rm sm^{-1}$) is the resistance per dry soil meter. Initially, it is equal to $33000 \rm sm^{-2}$ as introduced by Ducoudré et al. (1993).

New computation of evapotranspiration in SECHIBA

According to Boone et al. (2004), ET simulated by SECHIBA is underestimated compared with other LSMs and especially bare soil evaporation component. This weakness will appear in the results of simulations SECH1 to SECH4 described in section 5.2.1. Therefore, a new parameterization was implemented by D'Orgeval (2006) in the computation of water fluxes between soil, vegetation and atmosphere. This new parameterization will be tested in our study in simulations SECH5 and

SECH6. The evaporation of water intercepted by the cover is now computed over the total surface of the leaf. In a first approximation, each time the potential flux is not satisfied by evaporation of intercepted water, the transpiration of the vegetation ($T_{\mathrm{v}}^{\mathrm{new}}$, Eq. 16) takes over. It is constant as long as the sum of transpiration and evaporation of intercepted water is lower than potential evaporation.

$$T_{\mathrm{v}}^{\mathrm{new}} = \min\left[(I_{\mathrm{v}}^{\max} - I_{\mathrm{v}}), f_{\mathrm{v}}\left(\frac{1}{1+\frac{r_{\mathrm{s_v}}+r_{\mathrm{sto_v}}}{r_{\mathrm{a}}}}\right)U_{\mathrm{s_v}}E_{\mathrm{pot}}\right] \tag{16}$$

By this way, the sum of the evaporation of water intercepted by the leaves and the transpiration reaches faster the potential than in the previous parameterization. The total ET is consequently enhanced.

Furthermore, the bare soil evaporation (E_1^{new}, Eq. 19) is computed more realistically because a sub-fraction of bare soil uncovered by the vegetation (f_{v}^1) is estimated by an extinction coefficient ($e = 0.5$):

$$f_{\mathrm{v}}^1 = \exp(-e\mathrm{LAI_v}) \tag{17}$$

This sub-fraction will increase with the decrease of the LAI typically in autumn and consequently enables the evaporation of the bare soil under vegetation. A new fraction of bare soil f_1' is defined in the model:

$$f_1' = \sum_{\mathrm{v}=1}^{13} f_{\mathrm{v}}^1 f_{\mathrm{v}} \tag{18}$$

The bare soil evaporation is now computed over this new fraction:

$$E_1^{\mathrm{new}} = \min\left[f_1'\left(\frac{1}{1+\frac{r_1}{r_{\mathrm{a}}}}\right)U_{\mathrm{s_1}}E_{\mathrm{pot}}, E_{\mathrm{pot}} - \sum_{\mathrm{v}=2}^{13}(I_{\mathrm{v}} + T_{\mathrm{v}}^{\mathrm{new}})\right] \tag{19}$$

Root extraction

Transpiration of the cover is governed by the ability of the roots to extract water from the soil (Desborough, 1997). This phenomenon is represented by the term $U_{\mathrm{s_v}}$ in equations of ET (De Rosnay and Polcher, 1998). It decreases exponentially when dry soil depth increases in order to represent the potential of water extraction by the roots (Fig. 4). It is more or less significant according to the dry soil depth. When it rains, the superficial layer of the soil can be saturated and no dry soil layer is present: $h_{\mathrm{upper_v}}^{\mathrm{dry}} = 0\mathrm{m}$ and $U_{\mathrm{s_v}} = 1$. ET is consequently maximal (at the potential value weighted by a term of resistance) and the roots are more efficient in extracting water for transpiration. On the contrary, under dry conditions, the layer of dry soil ($h_{\mathrm{upper_v}}^{\mathrm{dry}}$) is formed and increases while $U_{\mathrm{s_v}}$ decreases exponentially approaching 0. The model simulates the difficulty for the roots to extract water all the more their density is low. In order to simulate the different intensity to extract water according to the PFT, different values of the parameter c_{v} have been attributed for each one. Therefore, a water extraction potential of roots $U_{\mathrm{s_v}}$ is computed for each PFT and for each soil layer. Two cases can be distinguished:

1. if the superficial reservoir of the soil does not exist, there is only one root extraction potential (Eq. 20)

2. if the superficial reservoir of the soil is present, one root extraction potential is distinguished for each reservoir (Eqs. 20 and 21) and the maximum between both is taken (Eq. 22). By this way, we favour the evaporation by the upper part of the root system whose efficiency in contributing water to transpiration is higher than lower roots (De Rosnay and Polcher, 1998).

$$U_{s_v}^{\text{lower}} = \exp\left(-c_v h_{\text{tot}} \frac{h_{\text{lower}_v}^{\text{dry}}}{h_{\text{tot}}}\right) \tag{20}$$

$$U_{s_v}^{\text{upper}} = \exp\left(-c_v h_{\text{tot}} \frac{h_{\text{upper}_v}^{\text{dry}}}{h_{\text{upper}_v}}\right) \tag{21}$$

$$U_{s_v} = \max\left(U_{s_v}^{\text{lower}}, U_{s_v}^{\text{upper}}\right) \tag{22}$$

3 Experimental design

The ability of the model SECHIBA to compute the water budget realistically at two different spatial scales is tested. In a first time, simulations with SECHIBA are performed over the US (Sect. 5.1) where mean annual ET (from initial computation in the model) and total runoff results are compared with four LSMs (NOAH (National Centers for Environmental Prediction, Oregon State, University Air Force, Hydrology Lab, Betts et al., 1997; Chen et al., 1997; Ek et al., 2003), VIC (Variable Infiltration Capacity LSM, Liang et al., 1994; Wood et al., 1997), MOSAIC (Koster and Suarez, 1994, 1996; Koster et al., 2000) and SAC (Sacramento Soil Water Accounting Model, Burnash et al, 1973; Burnash, 1995) during the numerical experiments performed in Mitchell et al. (2004). The simulations by the five models including SECHIBA have been performed over the time period 1st October 1997 to 30 September 1999 with the same NLDAS forcing dataset.

In a second time, the study is focused on the Illinois state (Sect. 5.2) where measurements of soil moisture content were initiated by the Illinois Water Survey (Hollinger and Isard, 1994). Initially, the distribution of vegetation in SECHIBA is prescribed by the vegetation map. This distribution is compared with the vegetation cover on which the measurements were performed. Each measurement station is associated with the corresponding grid cell of the model, according to the coordinate of the station (see Table 3 in Appendix) as in Fig. 5. The vegetation cover of the map differs from the one on which the measurements were performed (i.e. grass cover). Fig. 5a shows that few grid cells of the model are covered by grassland (grid cells containing stations 9, 11 and 82) and less than 10 % of their area is covered by this PFT. The prevailing type of vegetation over Illinois in the vegetation map is the PFT "C_3 crops" type. Eight grid cells containing stations are covered by the PFT "C_3 crops" at least by 90 % (no. 1, 5, 6, 8, 9, 13, 15 and 16) according to Fig. 5b. Consequently, a direct comparison cannot be established between results of integrated simulated soil moisture over the grid

cell and the measurements, until the proportion of one PFT is not above 90 %. So the first objective is to gradually transform "C_3 crops" PFT (that is prescribed in the model) in "C_3 grassland" PFT on these grid cells to be closer to the experimental conditions (Sect. 5.2.1). This allows a better agreement with the local characteristics of the vegetation cover on which the measurements were performed, and an evaluation of the weight of each parameters that have been modified in the model, on simulated soil moisture.

For the control simulation (SECH1, see Table 2), we start the study from the distribution of vegetation imposed by the vegetation map over the eight grid cells containing high proportion of "C_3 crops". First, gradual changes of crops parameters ($\mathrm{LAI}_{\mathrm{v}}^{\mathrm{max}}$ (SECH2, see Table 2), root extraction parameter c_{v} and crop height (SECH3, see Table 2)) are performed. Then, we prescribed "C_3 grassland" PFT over all the grid cells (SECH4, see Table 2) and a test of the new ET computation (see Sect. 2.2.3) is performed (SECH5, see Table 2) to be closely related to the experimental conditions over a grass cover. At each step, the accuracy to simulate more realistically the SWI seasonal variation is highlighted when compared to the Illinois in-situ observations database (described in sect. 4) over the 1997-1999 period. Secondly, the sensitivity of soil moisture to precipitation (SECH6, see Table 2) is studied (Sect. 5.2.2). Moreover, we test a different evaluation of field capacity from measurements (Sect. 5.2.3). Thirdly, a comparison of the total runoff simulated by the model with data over the Kaskaskia River basin in Illinois (see Fig. 1 for location) is performed (Sect. 5.3).

For both US and Illinois simulations, a four-year spin-up has been performed over the same year 1997 to reach a state of equilibrium under the applied forcing.

4 Soil moisture database

Soil moisture data used in this study is part of the Global Soil Moisture Database (Robock et al., 2000) which collect up to 15 yr in-situ recordings of soil moisture over more than 600 stations of many countries (such as Russia, China, Mongolia, India and US). The measurements in Illinois were performed with neutron probes, first at eight grass-covered sites in 1981 and then seven sites were added in 1982 and two more in 1986. Finally, since 1992, nineteen ICN stations (see Table 3 in Appendix) have collected data especially soil moisture and precipitation. Soil moisture measurements were established on eighteen grass-covered stations and one on bare soil over the time period 1981–2004. They were taken within 11 soil layers to a depth of two meters; the first in the top 0.1 m of the profile, then every 0.2 m from a depth of 0.1 m through 1.9 m, and the last in the layer between 1.9 m and 2.0 m. Each site was visited twice each month: the week of the 15th and the week of the last day of the month during March through September, and once each month during the last week of October through February (Hollinger and Isard, 1994). Excepted sand site at Topeka, silty loam (or silty clay loam for De Kalb and Champaign sites) is the predominant soil texture. In the 2-layer hydrology version of SECHIBA, soil texture is not taken into account so its impact on soil moisture

content cannot be studied here.

5 Results and discussion

5.1 Water balance simulated over US

According to Fig. 6, all the five models simulate the strong contrast between dried Western US where annual ET rate is generally less than $400\mathrm{mmyr}^{-1}$, and humid Eastern US where annual ET rate is able to reach $800\mathrm{mmyr}^{-1}$ and more. However, different patterns are simulated according the models. The patterns are similar over western region (excepted over California) between the models but differences in ET rate are shown between VIC (Fig. 6b) and SAC (Fig. 6d) or MOSAIC (Fig. 6c) of about 100 % over Eastern US. SECHIBA (Fig. 6e) simulates an ET similar to NOAH (Fig. 6a), the values being often between $600\mathrm{mmyr}^{-1}$ and $800\mathrm{mmyr}^{-1}$ over Eastern US for these two particular models. To establish the validity of the results, Mitchell et al. (2004) have used observed streamflow and annual discharges from 1145 basins and converted (using the basin area) to area-average mean annual runoff. They showed that mean annual runoff simulated by NOAH was in good agreement with runoff data over southern and northern part of Eastern US. Consequently, we conclude that ET rate simulated by NOAH is satisfying whereas VIC underestimates it (and overestimates runoff), contrary to MOSAIC and SAC which overestimate it. The fact that, over this region, ET rate distribution obtained with SECHIBA is similar to NOAH results is rather encouraging. Considering more precisely the Southeastern US region, we notice however that the ET rates simulated with SECHIBA are larger than with NOAH along the coast. This might be an improvement: actually, the study conducted by Mitchell et al. (2004) seems to show an overestimation of annual runoff and consequently an underestimation of ET rate. This difference is also found between NOAH and SECHIBA results over some parts of Northeast US, although SECHIBA remains more similar to NOAH than to the three other models. Moreover, according to Mitchell et al. (2004), NOAH and VIC overestimate the runoff rate over the state of Illinois (excepted for extreme northeast), the values being between 400 and $500\mathrm{mmyr}^{-1}$, whereas MOSAIC and SAC underestimate Illinois runoff (between 100 and $200\mathrm{mmyr}^{-1}$). It is quite satisfying that SECHIBA gives an intermediate runoff of about $300-400\mathrm{mmyr}^{-1}$ (not shown) compared to the other models. Orders of magnitude of ET and runoff simulated by SECHIBA seems to be satisfactory over United States and particularly in Illinois when compared to Mitchell et al. (2004). In the next section, in order to evaluate soil moisture, we focus our study on this state where many observations are available.

We note that after the completion of our study, a new comparison between observations and results from the same models has been published (Xia et al., 2012b). These new simulations have been performed where the accuracy and consistency of the forcing data have been increased (NLDAS-2), the four LSMs code upgraded and the study time period extended to 30 years (1979-2008) (Xia et al., 2012a). Contrasting results are obtained between this last study (Xia et al., 2012b) compared to the

previous ones (Mitchell et al., 2004). Xia et al. (2012b) found that Noah model overestimates mean annual runoff (and thus underestimates mean annual ET) as SAC and VIC results are the closest to the observations.

5.2 Soil moisture simulated over Illinois

5.2.1 Progressive and comprehensive adjustements of vegetation parameters

The comparison of the SWI between simulation and observations is first performed over the eight grid cells mentioned in Sect. 3. Over Illinois, the mean SWI computed from observed soil moisture (hereafter called "SWIo") at 8 stations (Observations 8s) shows a pronounced seasonality during the year according to Fig. 7a. It is maximal during winter and early spring reaching 0.80 in March during the period of low ET. The SWIo is decreasing during vegetation growth in spring to the middle of summer when climatic demand is maximal and thus water uptake by the vegetation significant. The SWIo remains low during autumn with values around 0.40. It shows a high variation during the three years in average over Illinois where a dry event occurs during the autumn 1999 and the SWIo value is less than 0.20 in November (Fig. 7b). This is due to the low precipitation occuring during this period over Illinois (less than $0.5\,\mathrm{mm\,d^{-1}}$ in November according to Fig. 2b).

SECHIBA does not reproduce the soil moisture seasonality when initial values of the vegetation parameters are used (SECH1 simulation, see Table 2). The soil is almost saturated throughout the year even during summer months where a decrease of only 10 % is simulated (Fig. 7a). SECHIBA does not capture well the amplitude of soil moisture variations with a variance (3.77×10^{-3}) largely underestimated compared to observations (29.1×10^{-3}). However, a seasonal variation is already noticed in agreement with observations (Fig. 7b). These remarks are confirmed over each of the eight grid cells (not shown).

Different hypothesis that could explain the global overestimation of the simulated SWI are successively highlighted and tested in this study. The parameters of vegetation of the model are gradualy changed to be closer to the experimental conditions. First, the parameterization of LAI is changed through two modifications (SECH2 simulation, see Table 2). The maximum value of LAI initially equal to 2.0 is increased to 3.5 which corresponds to a very high maximal value of LAI for grassland. Specific values of soil temperature determining the seasonality of the LAI are now included as described in Sect. 2.2.1. We obtain a seasonal variation of LAI closer to a grass cover expected in such a temperate region like Illinois: values are around zero during winter whereas LAI increases rapidly during April to reach maximal values in summer and early autumn (Fig. 8). The change of the minimum value of LAI was also tested but had no significant impact on soil moisture (not shown). In fact, during winter, ET is limited by the amount of incident energy and the impact of the vegetation cover is negligible. The effect of the LAI increase on soil moisture is not significant during winter (Fig. 7a) because the water uptake by the vegetation through transpiration is near zero

and only bare soil evaporation is occurring in SECH2 simulation (see Fig. 9). A higher decrease in soil moisture content compared to simulation SECH1 is found during late spring (Fig. 7a) due to the enhanced transpiration of the cover starting from the period of the vegetation growth (up to about $+0.3\mathrm{mm\,d^{-1}}$ in June for SECH2 compared to SECH1, not shown) converting more energy with a higher LAI. Moreover, plants intercept more precipitation (not shown). Thus, total ET is increased even more during summer but simulated SWI remains overestimated compared to observations with a mean relative error of variance greater than 80 %.

In order to improve the soil moisture seasonality and particularly its decrease during summer, the ability of the roots to extract the water from the soil is enhanced. Therefore, the parameter $c_{\mathrm{v}} = 4.0\mathrm{m^{-1}}$ is put to 1.0 (SECH3 simulation, see Table 2). The roots density is consequently increased allowing a higher transpiration (up to $+1.5\mathrm{mm\,d^{-1}}$ in July compared to SECH2 according to Fig. 9). The significant effect of the roots on the transpiration corroborates the result of Feddes et al. (2001) who showed that transpiration is more sensitive to the moisture content of a densely rooted soil layer. Moreover, De Rosnay and Polcher (1998) conclude that taking into account root profiles improves the representation of the seasonal cycle of transpiration. In our simulation, the roots have a strong impact on soil moisture content and improves the simulated SWI seasonal variation with a mean relative error of variance of 7 %. SWI mainly decreases during the period of vegetation in summer and autumn (up to 37.5 % in September compared to SECH2) (Fig. 7a). Simulated SWI is in better agreement with SWIo during autumn for the years 1997 and 1998 whereas the high decrease observed in 1999 is not pronounced enough in SECH3 (Fig. 7b). The results obtained during the dry season are different depending on the station. For example, at station 9, the pronounced decrease of the simulated SWI during autumn with SECH3 simulation compared to SECH2, induces a better capture of the soil dryness during this season when compared to the SWIo (Fig. 10a). However, the simulated seasonnality is poorly represented due to the soil moisture overestimation during spring in both simulations. At station 16, a lower decrease of the simulated SWI during spring induces a better seasonnality even a systematic overestimation of the simulated SWI throughout the year compared to the SWIo (Fig. 10b).

The height of SECHIBA vegetation is reduced from 1m to $30\,\mathrm{cm}$ which is more realistic to represent a grass cover. It has a little effect on soil moisture during autumn (up to 6 % of increase in October compared to SECH2, not shown) due to a slight decrease in ET (not shown), the surface of exchanges of the plant with its atmosphere being reduced.

SECHIBA simulates a low bare soil evaporation (Fig. 9) and no significant impact on soil moisture is found (up to about 3 % of decrease in March compared to SECH2, not shown) when the resistance of bare soil evaporation is tested (by dividing r_{soil} per 100). The results are quite similar over all the grid cells studied (not shown). This test shows that a value of $330\mathrm{s\,m^{-1}}$ for the resistance is already large enough to simulate the decrease of bare soil evaporation when soil moisture is low.

In conclusion, a grass cover rather realistic is thus simulated with SECH3 where the maximum

LAI is of 3.5 and the height of 30 cm. The sensitivity tests highlight the major impact of the roots extraction on soil moisture content in our model. The value of $c_{\mathrm{v}} = 1.0\mathrm{m}^{-1}$ allows more extraction of water from the first 50 cm of soil and soil moisture shows a higher decrease during spring and summer in agreement with reality. The other parameters as LAI and height of vegetation or soil resistance have a minor impact.

Another comparison is carried out that increases the sampling in order to improve the statistical study. A new simulation is performed (SECH4 simulation, see Table 2) where the parameterization of vegetation in SECH3 is kept but the same PFT is setting everywhere on the grid cells of SECHIBA. This allows us to include the results from all the grid cells containing the stations. This simulation is judicious as far as there is no feedback from the surface to the atmosphere. Thus, the impacts of the vegetation around the studied grid cells can be left. When all the same type of vegetation is set across the model grid, simulated soil moisture content remains overestimated compared to the new average of observations ("Observations 17 s") according to Fig. 11a. However, the seasonal variation is slightly improved compared to SECH3 with a mean relative error of variance of about 3.1 %. This improvement could be explained by the increase of the sampling improving the statistic for the simulation SECH4.

Bare soil evaporation simulated by SECHIBA is low. Thus, a new computation of ET which allows bare soil evaporation under the vegetation (see section 2.2.3) is implemented in the model (simulation SECH5, see Table 2). In this simulation, the parameterization of vegetation is the same than in SECH4. Global increase in ET simulated by SECH5 is low ($+8.0\%$) compared to SECH4, in average over the stations. Bare soil evaporation is now simulated throughout the year with SECH5, even when vegetation is present during summer (Fig. 12). As long as the total available energy to evaporate do not change between the two simulations, the transpiration of the cover decreases (evaporation of water intercepted by the cover does not change significantly). The global increase in ET has a significant impact on soil moisture when SECH5 is compared to SECH4. This change improves the seasonality of soil moisture (Fig. 11a). A decrease in soil moisture occurs throughout the year and particularly during autumn (up to 16 % of decrease in November). Simulated SWI is mainly improved compared to measurements during the autumn 1997 and 1998 whereas in autumn 1999 it remains overestimated (Fig. 11b).

In conclusion, the adjustement of the potential of water extraction by the roots and the implementation of the new computation of ET in the model are essential to simulate soil moisture in agreement with measurements at fine scale.

5.2.2 SWI variation according to precipitation data set

Precipitation dataset is crucial in soil moisture studies. As mentioned in section 2.1, we have found differences between NLDAS and in-situ observations. Thus, another evaluation of precipitation is tested in this study. NLDAS precipitation data is substituted by the in-situ precipitation, for each

station in the corresponding grid cell of the forcing grid. This allows an evaluation of a soil moisture sensitivity to precipitation variation. The impact on soil moisture is then studied with simulation SECH6 (see Table 2) including parameterization of vegetation and ET computation used in SECH5. Mean annual SWI simulated by SECHIBA forced by in-situ precipitation is decreased compared to SECH5 (Fig. 13) where NLDAS precipitation is higher than in-situ measurements (see Sect. 2.1). However, the decrease of simulated SWI occurs only during summer and autumn where it is now in good agreement with the SWIo (Fig. 13a) and particularly for the year 1998 (Fig. 13b). The overestimation of simulated SWI during the autumn 1999 is greatly reduced when in-situ precipitation is used. It is closer to the measurements which pointed out more dryness of the soil than the two previous years at the same time period (Fig. 13b). During winter and spring, SWI simulated with SECH6 slightly increases compared to SECH5 and remains systematically overestimated compared to the SWIo (Fig. 13a). This is also found for most of the stations (Fig. 14).

5.2.3 A different method to get measured field capacity

The estimation of field capacity measurement can be slightly different whether it is performed in laboratory or in-situ. Field capacity is usually measured in laboratory using "a pressure plate to apply a suction of $-1/3$ atmosphere to a saturated soil sample. When water is no longer leaving the soil sample, the soil moisture in the sample is determined gravimetrically and equated to field capacity." (Walker, 1989). Field method which consist in irrigating a test plot until the soil profile is saturated is particulary restrictive for this type of study. We suggest another method to measure the field capacity. It is considered as the maximal value of volumetric water in the soil during the year. Thus, we plot the monthly mean observed volumetric water profiles in average over the stations (Fig. 15) to deduce the field capacity: the maximal value of volumetric water during the year is obtained in March on the 30–50 cm layer of the soil (we consider that the 0–10 cm layer is not representative of the field capacity at monthly time scale). This value deduced from the volumetric water profile ($0.39\mathrm{kgm}^{-3}$) is lower than the measured field capacity ($0.41\mathrm{kgm}^{-3}$). The SWIo is then recomputed with the new value of field capacity (corresponding to "Observations 17 sfc" in Fig. 16) and its seasonality is compared to SECH6. The decrease of the field capacity in the re-computed SWIo leads to an increase of the observed SWI particularly during winter and spring. The simulated SWI from SECH6 becomes consequently closer to the re-computed SWIo during the three years with a better similarity in amplitude of the seasonality (Fig. 16).

5.2.4 Global analyze

To summarize in detail our results with simulation SECH6, the amplitude and the phase of the simulated SWI seasonality are represented for each station of Illinois (triangle) in the Taylor diagram (Taylor, 2001) (Fig. 17) which is frequently used in model evaluation studies. Overall, many stations show a simulated SWI in good agreement with the SWIo including field capacity correction when

SECHIBA is forced with in-situ precipitation and parameterized according to SECH6. Less than the half of the stations presents a relative error of SWI with observations around 10 % and less. SECHIBA captures quite well the phase of the SWI seasonality over Illinois (more than 80 % of stations shows a correlation greater than 0.85). The amplitude of SWI, which is very different according to the station, is much harder to capture (about 50 % of stations have a standard deviation of more or less 0.25 comparing to unit). Seasonality of simulated SWI at station 10 is the closest to the SWIo in term of amplitude (ratio of standard deviation is close to 1), phase (0.98 of correlation) and magnitude (17.5 % of relative error). SWI at station 13 is the worst simulated because of its low observed amplitude of SWI which SECHIBA cannot capture.

5.3 Simulated total runoff

The resulting total runoff simulated with SECH6 is compared with Kaskaskia streamflow data (divided by its corresponding basin surface) at Venedy station point (38°27′ N; 89°37′ W, Fig. 1), obtained from United States Geological Survey (USGS) for the period 1997–1999. This watershed is chosen because it integrates a large part of runoff over the south-west of Illinois. Runoff simulated with SECH6 is underestimated by 24 %. However, during the first half of the year, total runoff is well simulated (the mean relative error is about 2.5 % for the period January–May). SECHIBA reaches to capture the peak of runoff observed in March (Fig. 18). During the rest of the year, the simulated total runoff is null leading an underestimation in average over the year. This is partly due to the parameterization of the hydrological model which cannot produce runoff and drainage as far as simulated soil moisture does not reach field capacity. In the parameterization of the model used for simulation SECH6, the improvement of root extraction potential generates a level of soil moisture content always far from the field capacity during summer and consequently exacerbates the limitation of the hydrological modelling to simulate total runoff. The use of a multilayer approach to represent the vertical soil water diffusion (De Rosnay, 1999; De Rosnay et al., 2002) should be more satisfying to generate runoff and infiltration but it has not been tested in this study. However, underestimation of total runoff by SECHIBA can be due to the complexity of the water exchange between the deep soil and the surface through the water table that are included in the measurements datasets but not represented in the model.

6 Conclusions

This paper investigated the ability of SECHIBA to compute the surface water balance at two different spatial scales. At large scale (over the United States), ET and total runoff results from SECHIBA, forced by NLDAS at 1/8th degree resolution, are in good agreement with NOAH, considered as the closest to observations. At local scale (over Illinois), soil moisture content simulated by SECHIBA forced by the same dataset has been compared to observations from a global soil moisture database.

When vegetation parameters are defined by experimental conditions, the model is able to capture rather well the seasonal variation of soil moisture. The magnitude, amplitude and phase are well reproduced by the model over many stations. Uncertainties in climatic data, such as precipitation, that can induce a bias in the simulations of soil moisture, have been also pointed out. Extensions of this study could be performed such as the use of the new hydrological module or the dynamical vegetation to improve the simulation of soil moisture content. Moreover, the study of the impact of soil texture on soil moisture content is a reliable perspective to extend this study. The improvement of spatial resolution is a big challenge for climate modelling and particularly for the LSM which simulates land-use change. In this study, it is rather encouraging to obtain a realistic soil moisture seasonality at fine scale over Illinois with a global model such as SECHIBA which includes the simple hydrological model. Impact studies on water resources can be addressed with more confidence since soil moisture which has a crucial impact on water cycle, is well represented. For example, Guimberteau et al. (2011) simulated with SECHIBA coupled with LMDZ (Laboratoire de Météorologie Dynamique Zoom, Hourdin et al., 2006) a significant decrease in summer precipitation due to irrigation over the eastern part of the Mississippi River basin. Our comprehensive approach of gradual changes of the vegetation parameters over Illinois which is part of this region, can lead to a better understanding in the processes between the irrigated vegetation cover and climate.

Acknowledgements. We gratefully acknowledge Alan Robock to make available the soil moisture data bank of Illinois (Robock et al., 2000). We thank NLDAS team to make available NLDAS forcing dataset. We also thank the two scientific software engineers Martial Mancip and Patrick Brockmann (both IPSL) for their help about, respectively NLDAS forcing building for the SECHIBA model and for the fusion of the observed precipitation in NLDAS fields. Simulations have been performed using computational facilities of the Institut du Développement et des Ressources en Informatique Scientifique (IDRIS, CNRS, France).

The publication of this article is financed by CNRS-INSU.

References

Baldwin, M. E. and Mitchell, K. E.: The NCEP hourly multi-sensor U.S. precipitation analysis for operations and GCIP research, Preprints, 13th Conference on Hydrology, Long Beach, CA, Am. Meteorol. Soc., 54–55, 1997.

Belward, A., Estes, J., and Kline, K.: The IGBP-DIS global 1-km land-cover data set DISCover: a project overview, Photogramm. Eng. Rem. S., 5(9), 1013–1020, 1999.

Betts, A., Chen, F., Mitchell, K., and Janjic Z.: Assessment of the land surface and boundary layer models in two operational versions of the NCEP Eta model using FIFE data, Mon. Weather Rev., 125, 2896–2916, doi:10.1175/1520-0493(1997)125¡2896:AOTLSA¿2.0.CO;2, 1997.

Boone, A., Habets, F., Noilhan, J., Clark, D., Dirmeyer, P., Fox, S., Gusev, Y., Haddeland, I., Koster, R., Lohmann, D., Mahanama, S., Mitchell, K., Nasonova, O., Niu, G.-Y., Pitman, A., Polcher, J., Shmakin, A. B., Tanaka, K., van den Hurk, B., Vérant, S., Verseghy, D., Viterbo, P., and Yang, Z.-L.: The Rhone-Aggregation land surface scheme intercomparison project: an overview, J. Climate, 17(1), 187–208, 2004.

Budyko, M.I.: Heat Balance of the Earth Surface (in Russian), Gidrometeoizdat, St. Petersburg, Russia, 255pp., 1956.

Burnash, R. J. C., Ferral R. L., and McGuire R .A.: A generalized streamflow simulation system: Conceptual models for digital computer, technical report, Joint Fed. State River Forecast Cent., Sacramento, Calif., 1973.

Burnash, R. J. C.: The NWS river forecast system-catchment modeling, in Computer Models of Watershed Hydrology, edited by V. P. Singh, 311–366, Water Resour. Publ., Littleton, Colo., 1995.

Chen, T. H., Jankic, Z., and Mitchell, K.: Impact of atmospheric surface-layer parameterizations in the new land-surface scheme of the NCEP mesoscale Eta model, Boundary Layer Meteorol., 85, 391–421, doi:10.1023/A:1000531001463, 1997.

Cosgrove, B., Lohmann, D., Mitchell, K., Houser, P., Wood, E., Schaake, J., Robock, A., Marshall, C., Sheffield, J., Qingyuan, D., Lifeng, L., Higgins, R., Pinker, R., Tarpley, J., and Meng, J.: Real-time and retrospective forcing in the North American Land Data Assimilation System (NLDAS) project, J. Geophys. Res., 108(D22), 8842, doi:10.1029/2002JD003118, 2003.

De Rosnay, P. and Polcher, J.: Modelling root water uptake in a complex land surface scheme coupled to a GCM, Hydrol. Earth Syst. Sci., 2, 239–255, doi:10.5194/hess-2-239-1998, 1998.

De Rosnay, P.: Représentation de l'interaction sol-végétation-atmosphère dans le modèle de circulation générale du Laboratoire de Météorologie Dynamique thesis, State Univ. Pierre et Marie Curie, Paris VI, 176 pp., 1999.

De Rosnay, P., Polcher, J., Bruen, M., and Laval, K.: Impact of a physically based soil water flow and soil-plant interaction representation for modeling large-scale land surface processes, J. Geophys. Res.-Atmos., 107(D11), 4118, doi:10.1029/2001JD000634, 2002.

Desborough, C.: The impact of root weighting on the response of transpiration to moisture stress in land surface schemes, Mon. Weather Rev., 125(8), 1920–1930, 1997.

Dirmeyer, P., Zeng, F., Ducharne, A., Morrill, J., and Koster, R.: The sensitivity of surface fluxes to soil water content in three land surface schemes, J. Hydrometeorol., 1(2), 121–134, 2000.

D'Orgeval, T.: Impact du changement climatique sur le cycle de l'eau en Afrique de l'Ouest: modélisation et incertitudes, PhD thesis, Universite Paris VI, 2006.

Ducharne, A., Laval, K., and Polcher, J.:Sensitivity of the hydrological cycle to the parameterization of soil hydrology in a GCM, Clim. Dynam., 14, 307–327, 1997.

Ducoudré, N., Laval, K., and Perrier, A.: SECHIBA, a new set of parameterizations of the hydrologic exchanges at the land atmosphere interface within the LMD atmospheric global circulation model, J. Climate, 6(2), 248–273, 1993.

Dümenil, L., and Todini, E.: A rainfall-runoff scheme for use in the Hamburg climate model, In: J. O'Kane (ed.) Advances in theorical Hydrological Hydrology, A tribute to James Dooge, V.1 of European Geophysical Society Series on Hydrological Sciences,Elsevier, 129–157, 1992.

Ek, M. B., Mitchell K. E., Lin, Y., Rodgers, E., Grunman, P., Koren, V., Gayno, G., and Tarpley, J. D.: Implementation of Noah land surface model advances in the National Centers for Environmental Prediction operational mesoscale Eta model, J. Geophys. Res., 108(D22), 8851, doi:10.1029/2002JD003296, 2003.

Feddes, R., Hoff, H., Bruen, M., Dawson, T., De Rosnay, P., Dirmeyer, P., Jackson, R., Kabat, P., Kleidon, A., Lilly, A., and Pitman, A. J.: Modeling root water uptake in hydrological and climate models, B. Am. Meteorol. Soc., 82(12), 2797–2810, 2001.

Guimberteau, M.: Analyse et modifications proposées de la modélisation de l'irrigation dans un modèle de surface, Master's thesis, Université Paris VI and Laboratoire de Météorologie Dynamique Paris Jussieu, 2006.

Guimberteau, M.: Modélisation de l'hydrologie continentale et influences de l'irrigation sur le cycle de l'eau, PhD thesis, Université Paris VI and Laboratoire de Météorologie Dynamique Paris Jussieu, 2010.

Guimberteau, M., Laval, K., Perrier, A., and Polcher, J.: Global effect of irrigation and its impact on the onset of the Indian summer monsoon, Clim. Dynam., online first, doi:10.1007/s00382-011-1252-5, 2011.

Higgins, R., Shi, W., Yarosh, E., and Joyce, R.: Improved United States precipitation quality control system and analysis, NCEP/Climate Prediction Center Atlas, US Dept. of Commerce/Natl. Weather Serv. Natl. Oceanic and Atmos. Admin., Camp Springs, Md., 7, 40, 2000.

Hollinger, S. and Isard, S.: A soil-moisture climatology of Illinois, J. Climate, 7(5), 822–833, 1994.

Hourdin, F., Musat, I., Bony, S., Braconnot, P., Codron, F., Dufresne, J.-L., Fairhead, L., Filiberti, M.-A., Friedlingstein, P., Grandpeix, J.-Y., Krinner, G., LeVan, P., Li, Z.-X., and Lott, F.: The LMDZ4 general circulation model: climate performance and sensitivity to parametrized physics with emphasis on tropical convection, Clim. Dynam., 27(7), 787–813, 2006.

Koster, R., and Suarez, M.: The components of the SVAT scheme and their effects on a GCM's hydrological cycle, Adv. Water Resour., 17, 61-78, doi:10.1016/0309-1708(94)90024-8, 1994.

Koster, R., and Suarez, M.: Energy and water balance calculations in the Mosaic LSM, NASA Tech. Memo., NASA TM-104606, vol. 9, 60 pp., 1996.

Koster, R., Suarez, M., and Heiser, M. : Variance and predictability of precipitation at seasonal-to-interannual timescales, J. Hydrometeorol., 1, 26–46, doi:10.1175/1525-7541(2000)001¡0026:VAPOPA¿2.0.CO;2, 2000.

Liang, X., Lettenmaier, D. P., Wood, E. F., and Burges, S. J.: A simple hydrologically based model of land surface water and energy fluxes for GCMs, J. Geophys. Res., 99, 14,415–14,428, doi:10.1029/94JD00483, 1994.

Mitchell, K., Lohmann, D., Houser, P., Wood, E., Schaake, J., Robock, A., Cosgrove, B., Sheffield, J., Duan, Q., Luo, L., Higgins, R., Pinker, R., Tarpley, J., Lettenmaier, D., Marshall, C., Entin, J., Pan, M., Shi, W., Ko-

ren, V., Meng, J., Ramsay, B., and Bailey, A.: The multi-institution North American Land Data Assimilation System (NLDAS): utilizing multiple GCIP products and partners in a continental distributed hydrological modeling system, J. Geophys. Res.-Atmos., 109(D7), D07S90, doi:10.1029/2003JD003823, 2004.

Olson, J., Watts, J., and Allison, L.: Carbon in Live Vegetation of Major World Ecosystems (ORNL-5862), Environmental Sciences Division Publication, Oak Ridge National Lab., TN (USA), 1983.

Pinker, R., Tarpley, J., Laszlo, I., Mitchell, K., Houser, P., Wood, E., Schaake, J., Robock, A., Lohmann, D., Cosgrove, B., Sheffield, J., Duan, Q., Luo, L., and Higgins, R.: Surface radiation budgets in support of the GEWEX Continental-Scale International Project (GCIP) and the GEWEX Americas Prediction Project (GAPP), including the North American Land Data Assimilation System (NLDAS) Project, J. Geophys. Res.-Atmos., 108(D22), 8844, doi:10.1029/2002JD003301, 2003.

Polcher, J.: Etude de la sensibilité du climat tropical à la déforestation, PhD thesis, Université Paris VI and Laboratoire de Météorologie Dynamique Paris Jussieu, 1994.

Robock, A., Vinnikov, K., Srinivasan, G., Entin, J., Hollinger, S., Speranskaya, N., Liu, S., and Namkhai, A.: The global soil moisture data bank, B. Am. Meteorol. Soc., 81(6), 1281–1299, 2000.

Rowntree, P.R. and Lean, J.: Validation of hydrological schemes for climate models against catchment data, J. Hydrol., 155, 301–323, 1994.

Saleem, J. and Salvucci, G.: Comparison of soil wetness indices for inducing functional similarity of hydrologic response across sites in Illinois, J. Hydrometeorol., 3(1), 80–91, 2002.

Taylor, K.: Summarizing multiple aspects of model performance in a single diagram, J. Geophys. Res.-Atmos., 106(D7), 7183–7192, 2001.

Walker, W.: Guidelines for designing and evaluating surface irrigation systems, FAO, Rome, 1989.

Wood, E. F., Lettenmaier, D. P., Liang, X., Nijssen, B., and Wetzel, S. W.: Hydrological modeling of continental-scale basins, Annu. Rev. Earth Planet. Sci., 25, 279–300, doi:10.1146/annurev.earth.25.1.279, 1997

Xia, Y., Mitchell, K., Ek, M., Sheffield, J., Cosgrove, B., Wood, E., Luo, L., Alonge, C., Wei, H., Meng, J., Livneh, B., Lettenmaier, D., Koren, V., Duan, Q., Mo, K., Fan, Y., and Mocko, D.: Continental-scale water and energy flux analysis and validation for the North American Land Data Assimilation System project phase 2 (NLDAS-2): 1. Intercomparison and application of model products, J. Geophys. Res., 117(D3), D03109, 2012a.

Xia, Y., Mitchell, K., Ek, M., Cosgrove, B., Sheffield, J., Luo, L., Alonge, C., Wei, H., Meng, J., Livneh, B., Duan, and Lohmann, D.: Continental-scale water and energy flux analysis and validation for North American Land Data Assimilation System project phase 2 (NLDAS-2): 2. Validation of model-simulated streamflow, J. Geophys. Res., 117(D3), D03110, 2012b.

Table 1. List of atmospheric forcing variables in NLDAS used for this study.

Name	Description	Units
T_{air}	Two meters air temperature	K
Q_{air}	Two meters air specific humidity	kgkg^{-1}
Wind_N	Ten meters wind speed (u component)	ms^{-1}
Wind_E	Ten meters wind speed (v component)	ms^{-1}
P_{surf}	Surface pressure	Pa
$\mathrm{SW}_{\mathrm{down}}$	Surface downward short wave flux	Wm^{-2}
$\mathrm{LW}_{\mathrm{down}}$	Surface downward long wave flux	Wm^{-2}
Rainf	Rainfall rate	$\mathrm{kgm}^{-2}\mathrm{s}^{-1}$
Snowf	Snowfall rate	$\mathrm{kgm}^{-2}\mathrm{s}^{-1}$

Table 2. List of the simulations performed with their numerical settings. Red color indicates the changed value of a parameter compared to the previous parameterization.

Simulations	$T_{soil_{\mathrm{v}}}^{min}$;$T_{soil_{\mathrm{v}}}^{max}$ (°C)	LAI_{v}^{min};LAI_{v}^{max}	h (m)	c_{v} (m^{-1})	r_{soil} ($s.m^{-2}$)	Number of grid cells for average	Bare soil evaporation under vegetation	Precipitation forcing
SECH1	0;20	0;2.0	1.0	4.0	33000	8	No	NLDAS
SECH2	7;15	0;3.5	1.0	4.0	33000	8	No	NLDAS
SECH3	7;15	0;3.5	1.0	1.0	33000	8	No	NLDAS
-	7;15	0;3.5	0.3	1.0	33000	8	No	NLDAS
-	7;15	0;3.5	0.3	1.0	330	8	No	NLDAS
SECH4	7;15	0;3.5	0.3	1.0	330	17	No	NLDAS
SECH5	7;15	0;3.5	0.3	1.0	330	17	Yes	NLDAS
SECH6	7;15	0;3.5	0.3	1.0	330	17	Yes	In-situ

Table 3. List of measurements stations with their references (number, site code, coordinates and elevation). We do not take into account stations 2 and 17 for the present study.

Number	Name	Site code	Latitude (N)	Longitude (W)	Elevation (m)
1	Bondville	BVL	40°03′	88°52′	213
2^{+}/82	Dixon Springs (bare^{+}/grass)	DXG	37°27′	88°40′	165
3	Brownstown	BRW	38°57′	88°57′	177
4	Perry	ORR	39°48′	90°50′	206
5	De Kalb	DEK	41°51′	88°51′	265
6	Monmouth	MON	40°65′	90°41′	229
8	Peoria	ICC	40°42′	89°32′	207
9	Springfield	LLC	39°31′	89°37′	177
10	Belleville	FRM	38°31′	89°53′	133
11	Carbondale	SIU	37°43′	89°14′	137
12	Olney	OLN	38°44′	88°06′	134
13	Freeport	FRE	42°14′	89°40′	265
14	Ina	RND	38°08′	88°55′	130
15	Stelle	STE	40°25′	89°19′	207
16	Topeka	MTF	40°18′	89°54′	152
17*	Oak Run	OAK	40°58′	90°09′	265
34	Fairfield	FAI	38°23′	88°23′	136
81	Champaign	CMI	40°07′	88°14′	219

* Missing data for 1998 and 1999 for this station

$^{+}$ Measurements performed over bare soil for this station.

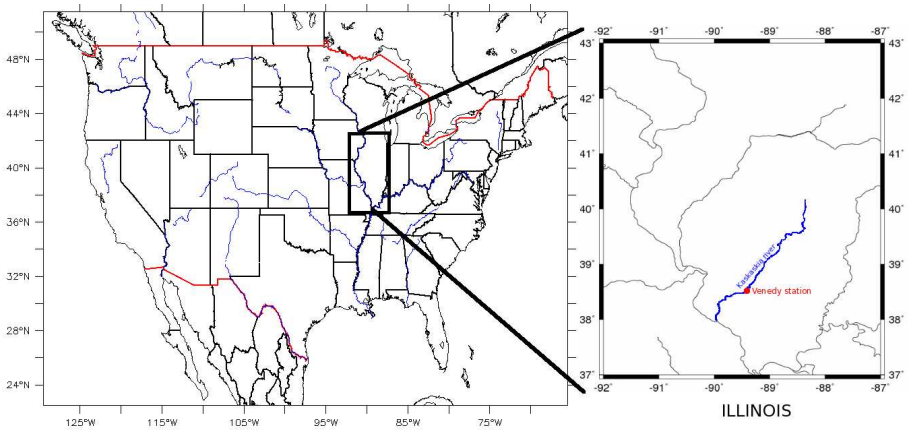

Fig. 1. Location of the Illinois state. Kaskaskia river and Venedy station are also localized.

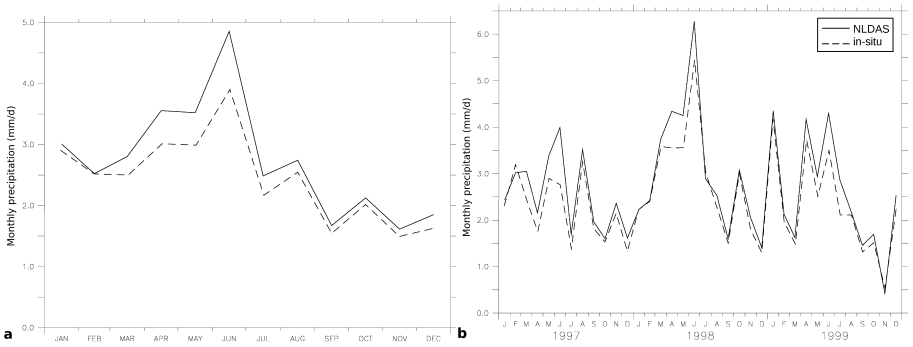

Fig. 2. Monthly mean **(a)** and monthly **(b)** precipitation (mmd^{-1}) for NLDAS (black line) and in situ data (dashed line), for 1997-1999

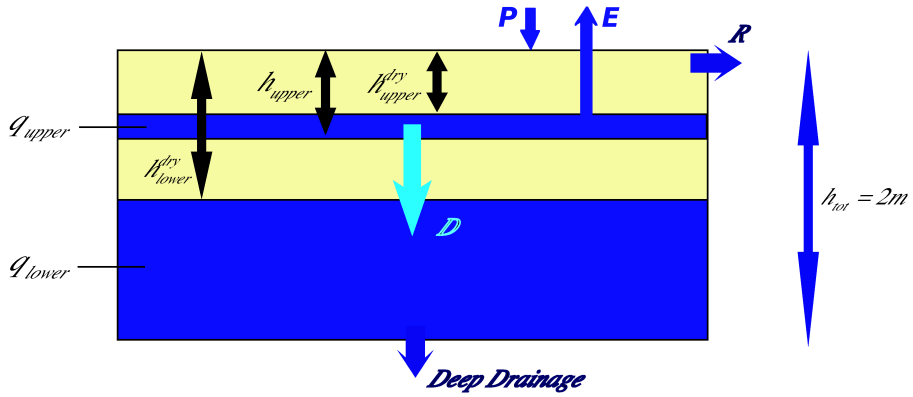

Fig. 3. Scheme of the soil with hydrology in SECHIBA. q_{upper} and q_{lower} (both in kgm^{-2}) are, respectively the amount of water available for the plants contained in the upper and lower reservoir, $h^{\mathrm{dry}}_{\mathrm{upper}}$ and $h^{\mathrm{dry}}_{\mathrm{lower}}$ (both in m) the depths of dry soil layers, respectively over the superficial and the deep soil reservoir, h_{upper} (m) is the height of the superficial reservoir, R the runoff at the surface, D ($\mathrm{kgm}^{-2}\mathrm{s}^{-1}$) the drainage between the two soil layers, E ($\mathrm{kgm}^{-2}\mathrm{s}^{-1}$) the total evaporation and P ($\mathrm{kgm}^{-2}\mathrm{s}^{-1}$) the precipitation

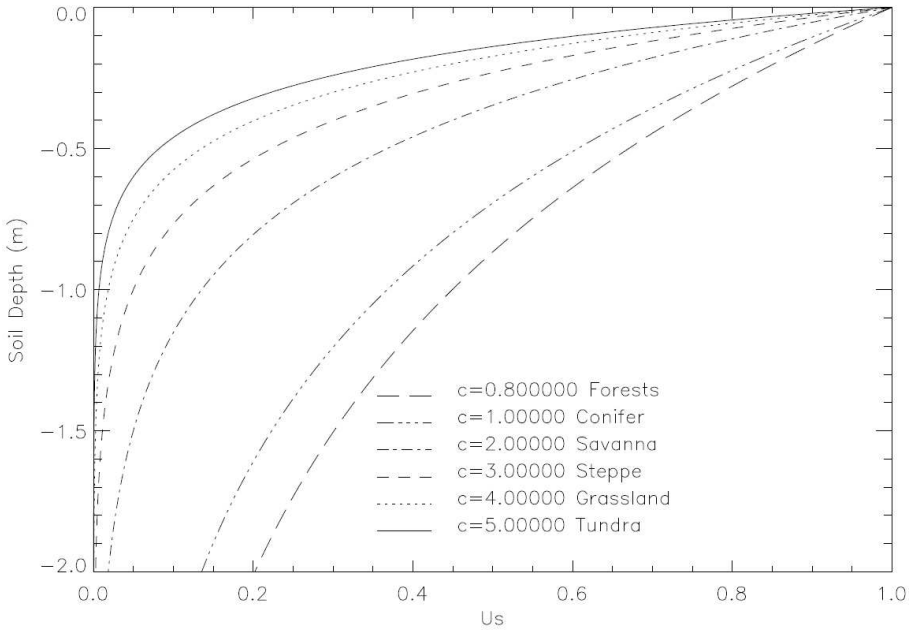

Fig. 4. Water uptake function, U_{s_v}, for each canopy (De Rosnay and Polcher, 1998). The profiles depend on the depth of the dry soil and the value of the constant c_v.

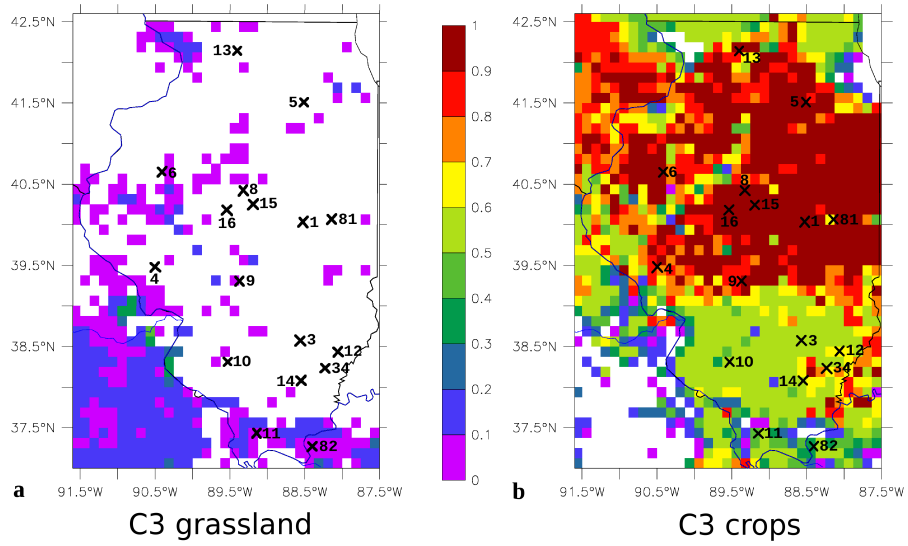

Fig. 5. Fraction of PFT **(a)** "C_3 grassland" and **(b)** "C_3 crops" covers on each grid cell across Illinois prescribed by the vegetation map in SECHIBA. The 17 stations used for this study are indicated on the figure (see Table 3 in Appendix for their references).

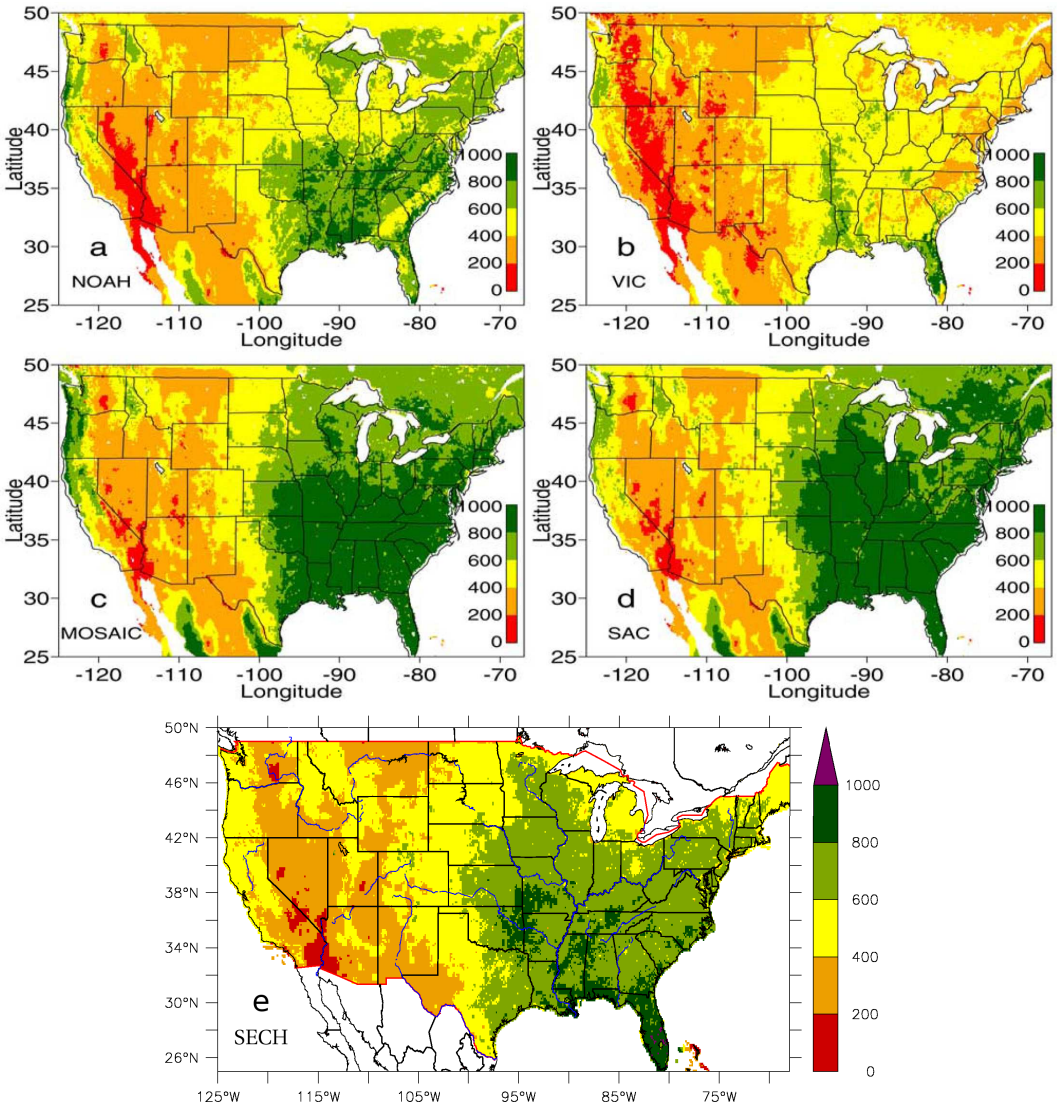

Fig. 6. Mean annual ET ($\mathrm{mm yr}^{-1}$) over the United States, for the mean time period 1 October 1997–30 September 1999, from **(a)** NOAH, **(b)** VIC, **(c)** MOSAIC **(d)** SAC and **(e)** SECHIBA. The first four maps were taken from Mitchell et al. (2004).

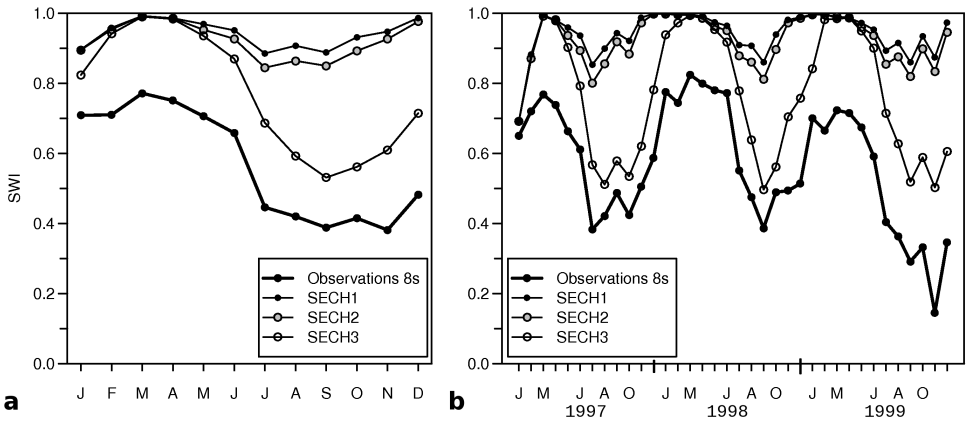

Fig. 7. Monthly mean SWI averaged over the eight selected stations, from observations and simulations SECH1 to SECH3. **(a)** Averaged seasonal cycles and **(b)** time series over the time period 1997–1999.

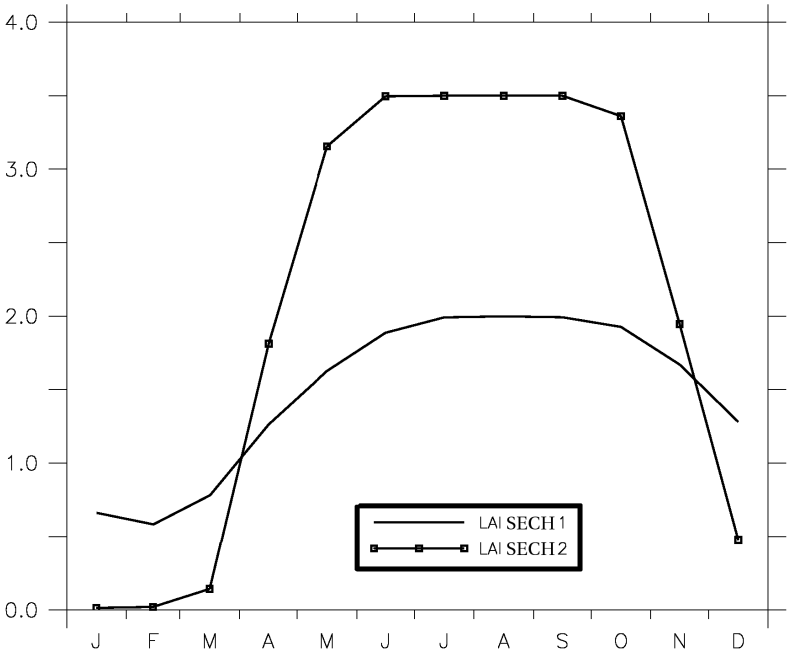

Fig. 8. 1997-1999 mean LAI seasonal cycle simulated from SECH1 and SECH2, averaged for the 8 validation grid cells (see Sect. 3).

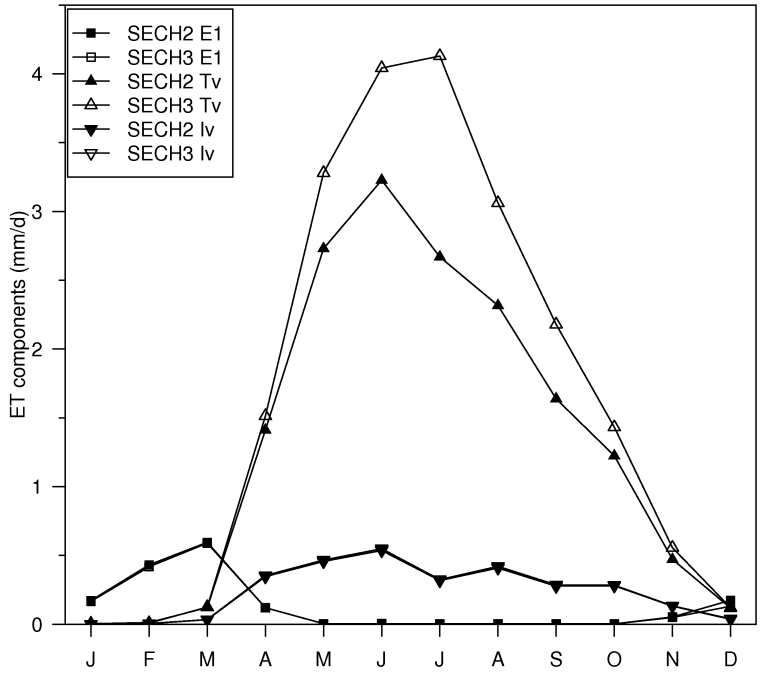

Fig. 9. Seasonal cycles of monthly mean ET components (sublimation not shown) ($\mathrm{mm\,d^{-1}}$) averaged over the eight selected grid cells, from SECH2 and SECH3, for the mean time period 1997–1999. ET components are E_1 (bare soil evaporation), Tv (transpiration) and Iv (evaporation of water intercepted by the cover).

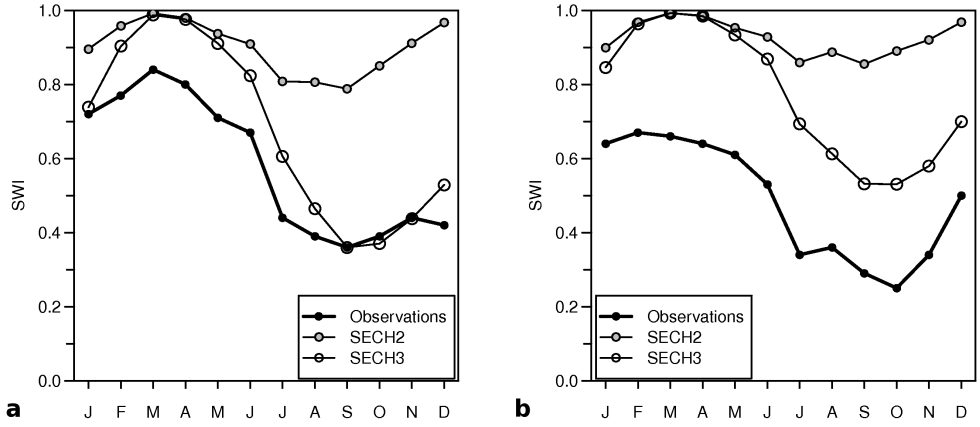

Fig. 10. Seasonal cycles of monthly mean SWI on **(a)** station 9 and **(b)** station 16, from observations and simulations SECH2 and SECH3, for the mean time period 1997–1999.

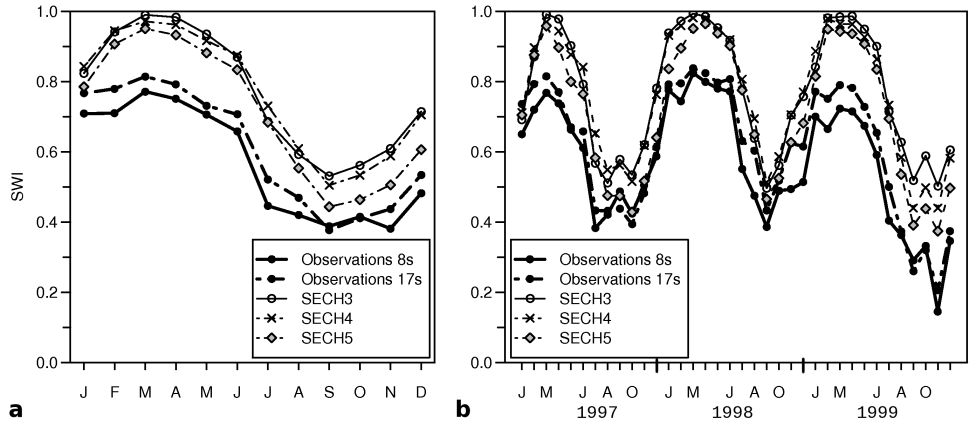

Fig. 11. Monthly mean SWI averaged over all the stations, from observations and SECH3 to SECH5. **(a)** Averaged seasonal cycles and **(b)** time series over the time period 1997–1999.

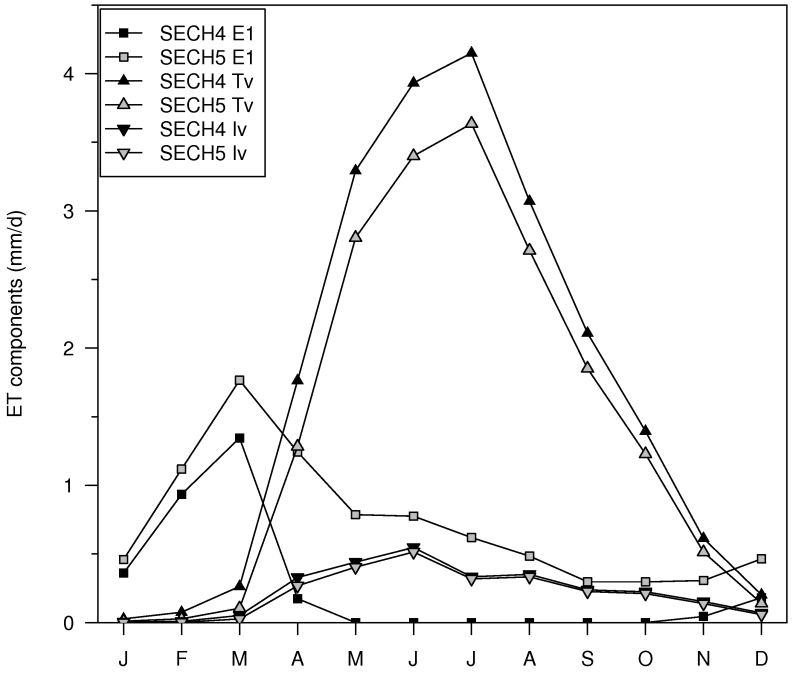

Fig. 12. Seasonal cycles of monthly mean ET components (sublimation not shown) ($\mathrm{mm\,d^{-1}}$) averaged over all the selected grid cells, from SECH4 and SECH5, for the mean time period 1997–1999. ET components are E_1 (bare soil evaporation), Tv (transpiration) and Iv (evaporation of water intercepted by the cover).

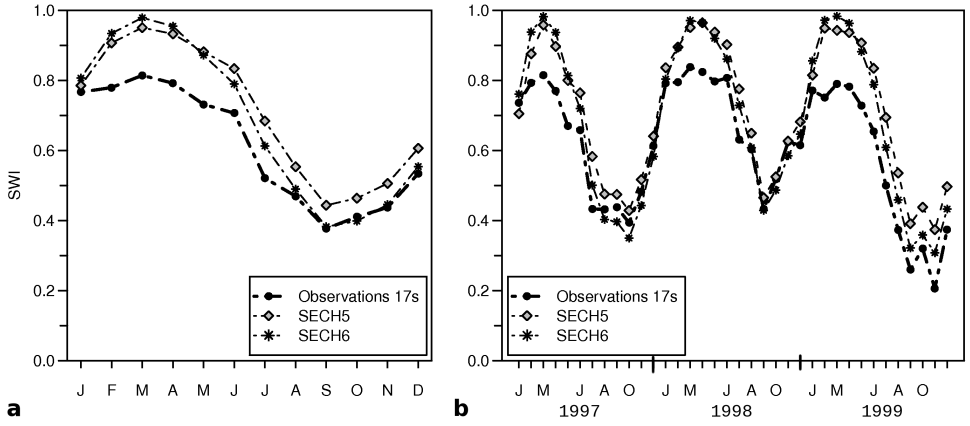

Fig. 13. Monthly mean SWI averaged over all the stations, from observations, SECH5 and SECH6. **(a)** Averaged seasonal cycles and **(b)** time series over the time period 1997–1999.

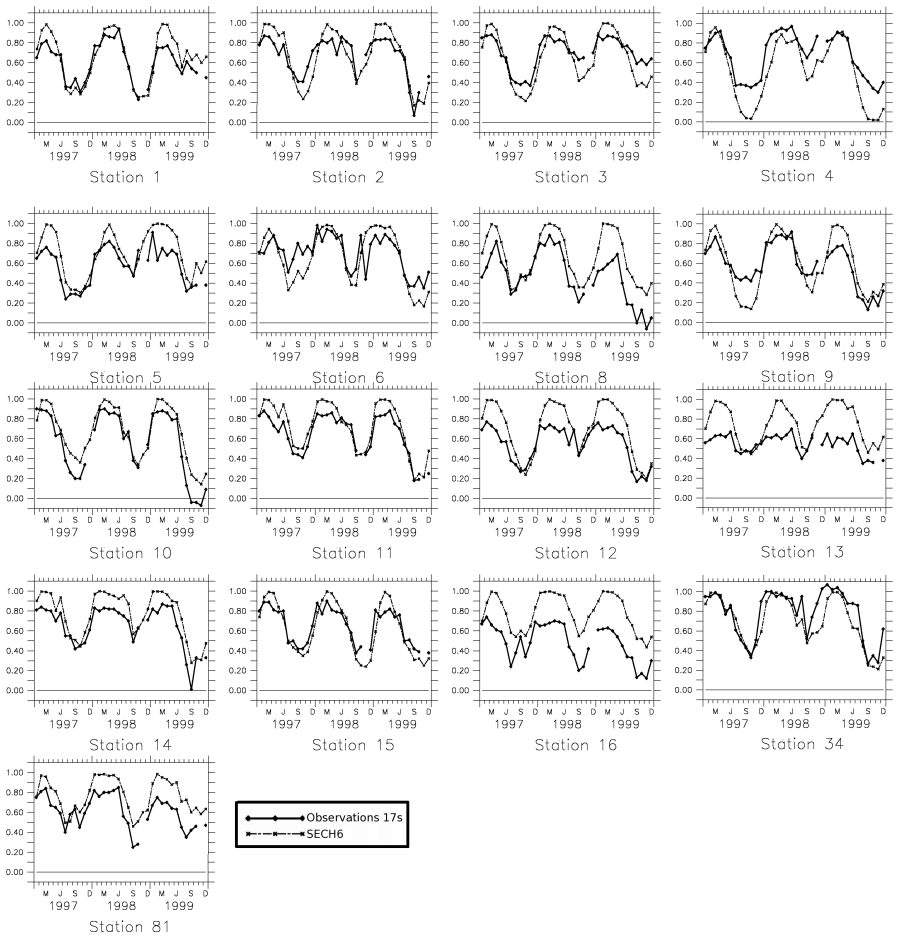

Fig. 14. Times series of monthly mean SWI for each studied stations, from observations and SECH6, for the time period 1997–1999.

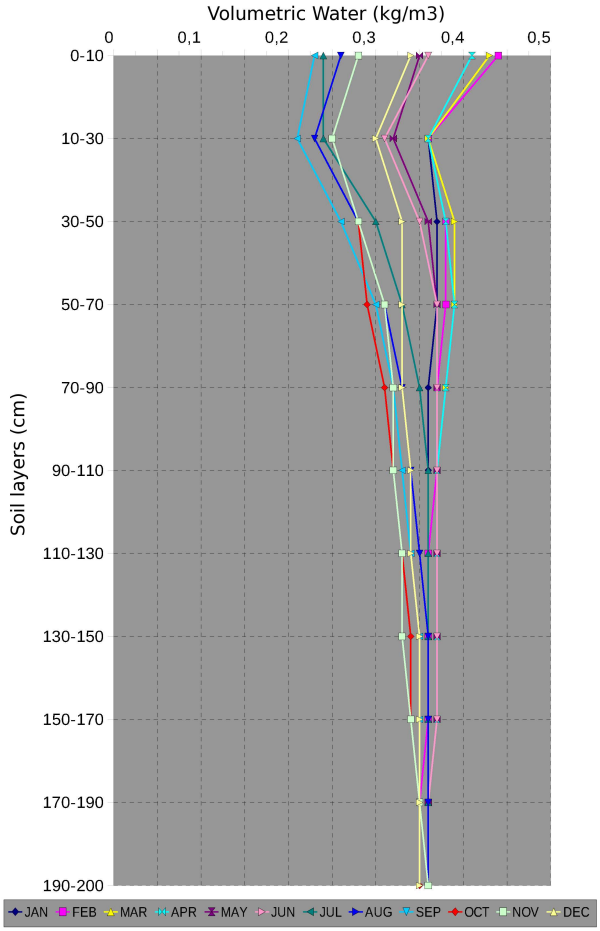

Fig. 15. Monthly mean volumetric water profiles averaged over all the stations, for the mean time period 1997–1999.

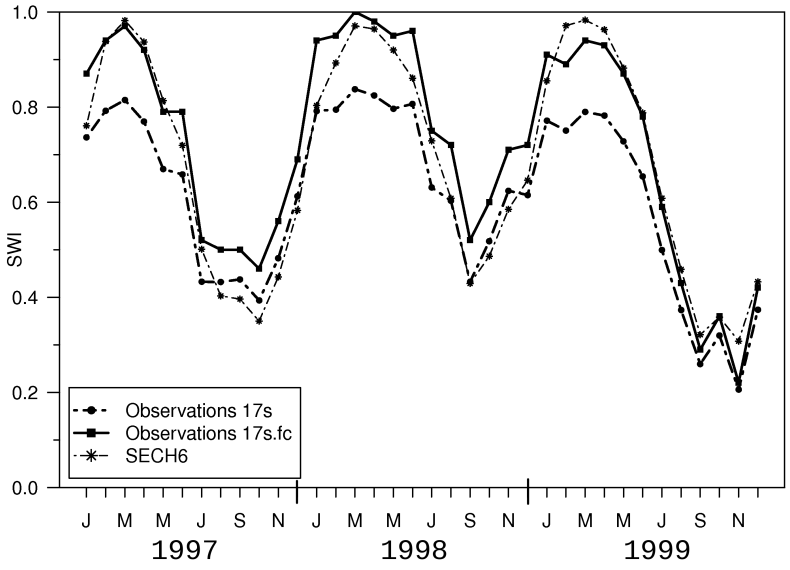

Fig. 16. Times series of monthly mean SWI averaged over all the stations, from observations, new profile of observations and SECH6, for the time period 1997–1999.

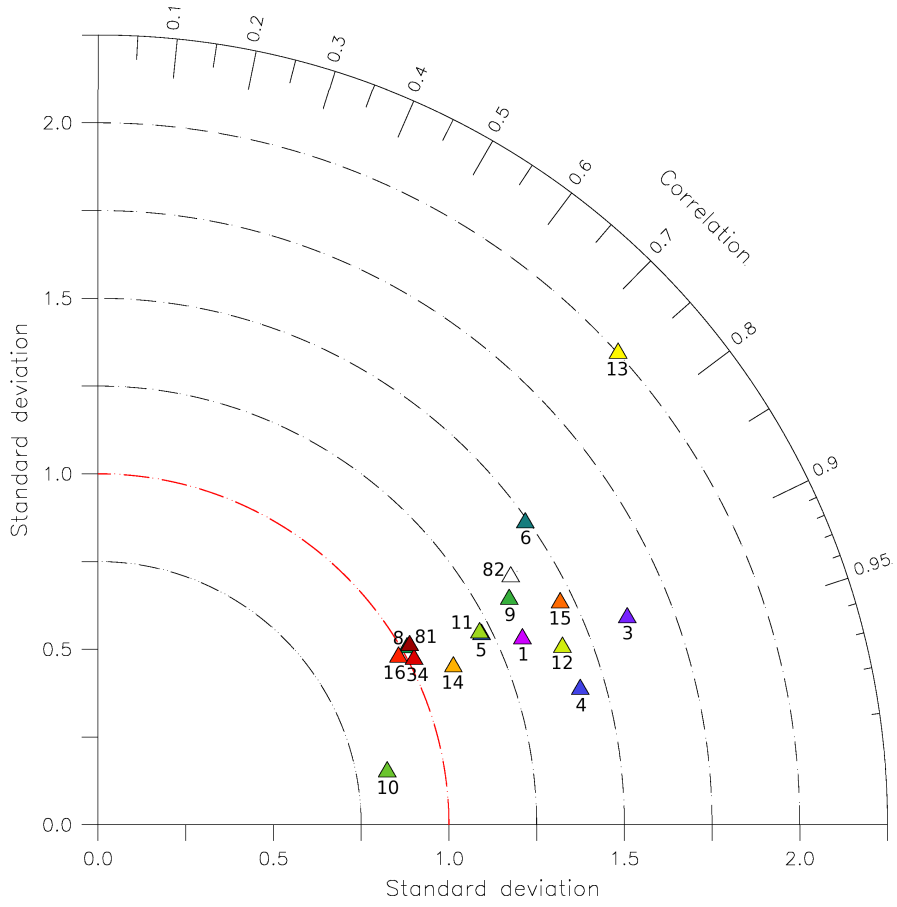

Fig. 17. Taylor diagram illustrating the statistics of SWI simulated with SECH6, from 1997 to 1999. Each station is represented by a colored triangle with its number. The Taylor diagram is a representation that provides the ratio of the simulated and the observed standard deviation as a radial distance from the origin and the correlation of simulated SWI with observations as the cosine of the azimuth angle in a polar plot. R correlation coefficient is computed according to the following equation: $R = \frac{\frac{1}{N}\sum_{n=1}^{N}\left(Q_n^{\mathrm{ORCH}} - \overline{Q^{\mathrm{ORCH}}}\right)\left(Q_n^{\mathrm{OBS}} - \overline{Q^{\mathrm{OBS}}}\right)}{\sigma_{Q^{\mathrm{ORCH}}}\sigma_{Q^{\mathrm{OBS}}}}$ where n is the month $(1 < n < N = 36)$, Q^{ORCH} and Q^{OBS} are, respectively simulated and observed monthly mean SWI and $\sigma_{Q^{\mathrm{ORCH}}}$ and $\sigma_{Q^{\mathrm{OBS}}}$ are, respectively simulated and observed standard deviations. The mean SWIo averaged over all the stations is plotted at (1,0): no error in standard deviation and zero correlation error. The distance between the point (1,0) and the simulated result point is proportional to the root mean squared error. Good representation of the amplitude simulated by the model compared to observations is traduced by a triangle close to the dashed red line as radial distance. Good representation of the phase is traduced by a short distance between the triangle and the unit on the abscissa axis.

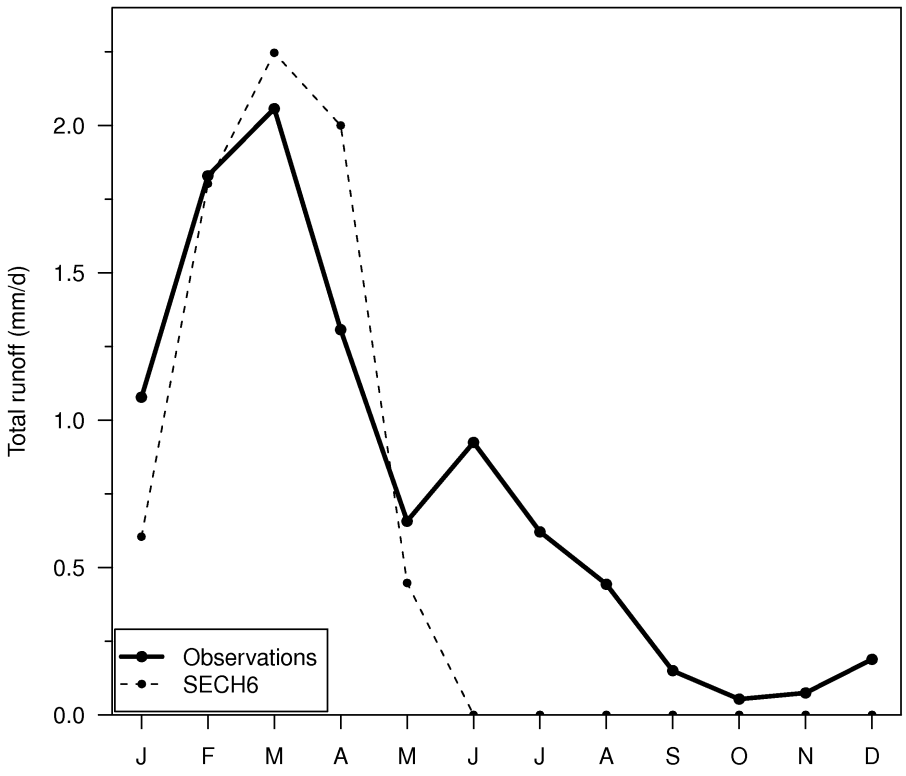

Fig. 18. Seasonal cycles of monthly mean total runoff (mmd^{-1}) on the grid cell corresponding to Venedy station coordinates, from observations and SECH6, for the mean time period 1997–1999.